An Improved Algorithm for Retrieving Surface Downwelling Longwave Radiation from Satellite Measurements

Yaping Zhou[1], David P. Kratz[2], Anne C. Wilber[3], Shashi K.Gupta[3] and Robert D. Cess[4]

[1]Goddard Earth Sciences & Technology Center, University of Maryland Baltimore County, Catonsville, MD

[2]Climate Science Branch, NASA Langley Research Center, Hampton, VA

[3]Analytical Services & Materials, Inc., Hampton, VA

[4] Marine Sciences Research Center, S.U.N.Y. at Stony Brook, Stony Brook, NY

Submitted to Journal of Geophysical Research

November, 2006

Corresponding author address: Dr. Yaping Zhou, Mail code 613.2, NASA Goddard Space Flight Center, Greenbelt, MD 20771. Email: yzhou@climate.gsfc.nasa.gov

Abstract Zhou and Cess [2001] developed an algorithm for retrieving surface downwelling longwave radiation (SDLW) based upon detailed studies using radiative transfer model calculations and surface radiometric measurements. Their algorithm linked clear sky SDLW with surface upwelling longwave flux and column precipitable water vapor. For cloudy sky cases, they used cloud liquid water path as an additional parameter to account for the effects of clouds. Despite the simplicity of their algorithm, it performed very well for most geographical regions except for those regions where the atmospheric conditions near the surface tend to be extremely cold and dry. Systematic errors were also found for scenes that were covered with ice clouds. An improved version of the algorithm prevents the large errors in the SDLW at low water vapor amounts by taking into account that under such conditions the SDLW and water vapor amount are nearly linear in their relationship. The new algorithm also utilizes cloud fraction and cloud liquid and ice water paths available from the Cloud and the Earth's Radiant Energy System (CERES) single scanner footprint (SSF) product to separately compute the clear and cloudy portions of the fluxes. The new algorithm has been validated against surface measurements at 29 stations around the globe for Terra and Aqua satellites. The results show significant improvement over the original version. The revised Zhou-Cess algorithm is also slightly better or comparable to more sophisticated algorithms currently implemented in the CERES processing and will be incorporated as one of the CERES empirical surface radiation algorithms.

1. Introduction

Using detailed studies based upon radiative transfer model calculations and surface radiometric measurements, Zhou and Cess [2001] formulated algorithm development strategies for retrieving surface downwelling longwave radiation (SDLW). Their studies demonstrated that clear sky SDLW could be largely determined by surface upwelling longwave flux and column precipitable water vapor. For cloudy sky cases, they used cloud liquid water path as an additional parameter to account for the effects of clouds instead of using cloud base height which is theoretically a more direct factor in determining the SDLW. An illustrative algorithm was derived and tested using observational data from Atmospheric Radiation Measurements (ARM) Program [Stokes and Schwartz 1994] measurements at the U.S. Southern Great Plain (SGP) and Tropical Western Pacific (TWP) sites.

Since the algorithm was derived and tested for mid-latitude and tropical conditions, there was concern that the algorithm might not perform well for extremely cold and dry conditions. Indeed, once data had become available from the ARM North Slope of Alaska (NSA) [Stamnes et al., 1999], large biases were found when the algorithm was applied to surface measurements from that location. Sensitivity studies demonstrated that the algorithm significantly underestimates SDLW when atmospheric water vapor was low.

Meanwhile, the Clouds and the Earth's Radiant Energy System [CERES; Wielicki et al. 1996] Surface Radiation Budget (SRB) team started to test the algorithm for possible global application. The CERES program is designed to provide crucial cloud and radiation measurements for studying cloud-radiation interaction. CERES instruments

were launched aboard the Tropical Rainfall Measuring Mission (TRMM) in November 1997 and on the Earth Observation System (EOS) Terra satellite in December 1999 and Aqua satellite in 2002. The space-borne CERES radiometers provide broadband total, shortwave (SW) and infrared window measurements at the top of atmosphere (TOA). Differencing the SW from the total measurements allows for a derivation of the longwave (LW) value. Deriving reliable estimates of SRB parameters is another important objective of the CERES project whose goal is to provide a complete picture of the energy budget of the earth–atmosphere system. Since the SRB cannot be directly measured by satellite-borne instruments, the surface fluxes are derived with several different methods using combinations of radiation models, data assimilation products, and satellite measurements. The Surface and Atmospheric Radiation Budget [SARB; Charlock et al. 1997] component of CERES represents one such method where shortwave and longwave fluxes at the surface, at three levels in the atmosphere, and at the TOA are computed with a radiative transfer model. In addition to SARB, surface fluxes are being derived within CERES using two SW and two LW models, which are based on TOA-to-surface transfer algorithms or fast radiation parameterizations. These models are the Li et al. [1993] model (SW model A, clear sky only), the Darnell et al. [1992] model (SW model B), the Inamdar and Ramanathan [1997] model (LW model A, clear sky only), and the Gupta et al. [1992] model (LW model B). These models were incorporated into CERES products to provide independent sources of surface fluxes to compare with SARB results [Gupta et al. 2004]. The Zhou-Cess algorithm represents a new methodology for deriving SDLW globally for both clear sky and cloudy sky using parameters readily available from satellite measurements. A vigorous test was performed on instantaneous flux derived by

Zhou-Cess algorithm as part of single-scanner footprints (SSF) products on board Terra and Aqua satellite against matched ground measurements from surface radiation measurement sites around the globe. Despite the simplicity of their algorithm, it performed very well for most of the geographical regions. Large biases, however, were found for certain regions, most notably the Polar Regions, where the atmosphere is extremely cold and dry. In addition, systematic errors were found for regions covered with ice clouds.

The modifications to the algorithm discussed in the present work are aimed at addressing the low water vapor and ice cloud situations with the goal of making the algorithm applicable for global implementation in the CERES processing. In section 2, a brief description of the original algorithm will be given followed by bias analysis of the algorithm when applied to ARM NSA data. In section 3, the algorithm is revised using collocated CERES cloud parameters and surface radiation measurements. The new algorithm is validated for CERES Terra and Aqua satellites with surface measurements from global network. A summary of this work is given in section 4.

2. Low Water Vapor Bias

2.1 Original algorithm

The Zhou-Cess algorithm took the form:

$$SDLW = a + b \bullet SULW + c \bullet ln(PWV) + d \bullet [ln(PWV)]^2 + e \bullet ln(1 + f \bullet LWP) \quad (1)$$

where SULW is the surface upwelling longwave flux computed from the 2-meter air temperature using Stefan-Boltzmann's law assuming an emissivity equal to unity. PWV is the column precipitable water vapor and LWP is the cloud liquid water path, both in

centimeters. The regression coefficients a, b c, d, e, f have values of 123.86, 0.444, 56.16, -3.65, 5.30, 1226.0, respectively. The algorithm was formulated based on detailed studies of radiative transfer models and observational data. The unique feature of this algorithm is that it uses one formula to compute the clear sky and all sky SDLW. The LWP is used as a surrogate of cloud base height since LWP is found to be correlated with cloud base height based upon observational data and upon thermodynamic arguments by Hack [1998]. LWP is also better defined for any spatial and temporal grid. The algorithm was derived using observational data obtained from six Intensive Observation Periods (IOP) at the ARM SGP site and was verified with nine other SGP IOP datasets and TWP Manus data [Zhou and Cess 2001]. The algorithm was not tested with observational data from other geophysical regions because of data availability problems.

2.2 The ARM NSA data

Recent climate modeling and diagnostic studies indicate the Polar Regions are particularly sensitive to global climate change and important to mid-latitude climate and weather systems [Stamnes et al., 1999]. Radiation tends to dominate the Arctic heat budget in all seasons. Due to the extreme weather conditions experienced at high latitudes, the algorithms developed for mid-latitudes frequently do not work well for the Polar Regions. Thus, prudence necessitated testing the Zhou-Cess algorithm once high quality observations from ARM NSA became available. The data used in the study was from January to December, 2000 from the ARM Barrow facility, which is located at the northernmost point (71.32^{o}N, 156.61^{o}W) in the United States, 528 km north of the Arctic Circle. The data were taken from the same instruments and processed in the same manner

as those used by Zhou and Cess [2001] for the SGP and TWP sites. The SDLW fluxes were pygeometer measurements and the surface upwelling fluxes were computed from the Surface Meteorological Observation Station (SMOS) 2-m surface air temperature. The column precipitable water and cloud liquid water were both measured by microwave radiometers (MWR). All data were averaged into half-hour products. The results show that the algorithm mostly underestimates the SDLW, with large negative bias at the low SDLW (Fig. 1). Further analysis found that 94% of the underestimated cases are related to very low water vapor amount (PWV < 0.81 cm). The low water vapor amount has resulted in very large negative value in the ln(PWV) term since the logarithmic function decreases very rapidly with decreasing water vapor below 1 cm. To remedy the problem, the ln(PWV) term was replaced by ln(1+PWV) to approximate a near-linear relationship between PWV and SDLW when water vapor amounts are very low. This modification has the added advantage of producing a very simple and reasonable relationship between the SDLW and the water vapor term which prevents the PWV from producing a negative contribution to the flux as the water vapor amounts asymptote toward zero.

Although Zhou and Cess [2001] conducted radiative transfer calculations for 6 default Moderate-Resolution Transmittance Radiation Model (MODTRAN, Wang et al. 1996) atmospheres (including subarctic summer and subarctic winter atmosphere) and their variations for providing basic relationships between SDLW and other parameters, the actual algorithm was derived using only observations at SGP site for illustrative purpose. For any nonlinear relationship, accounting for the full range of conditions is critical to derive statistical relationships that apply to most situations. This is because the statistical relations (usually derived with least square fitting) will lean toward highly

sampled situations and miss the under-sampled situations.

The importance of sampling can be illustrated in Fig. 2 where a linear relationship is calculated for MODTRAN computed SDLW and SULW from Zhou and Cess [2001] (upper panel). Using the upper portion (PWV>=0.5 cm) and the lower portion (PWV < 0.5 cm) of the data gives very different slope and offset for a linear relationship. The log-square fit of PWV to the ratio of fluxes also depends significantly on different portions of the sampling data (lower panel). The reason why the SGP algorithm does not produce good results for NSA data is because SGP data only represent middle range of the data, and thus, is not applicable to the low end of the curve. Fig. 3 illustrates the probability distribution functions (PDF) of SULW, SDLW and PWV from global networks of 29 sites (Fig. 4) and those from ARM SGP and NSA sites. An examination of Fig. 3 reveals that the dynamical range of surface longwave fluxes and PWV from SGP miss a small fraction of data where SULW is larger than 500 Wm^{-2} or PWV greater than 5 cm as shown in the global PDFs. More importantly, however, the NSA PDFs clearly demonstrate that the distributions of these quantities largely misrepresent regions of extremely cold and dry areas. The misrepresentation of low water vapor situations is particularly serious because of nonlinear logarithmic relationship between water vapor and SDLW.

Due to data availability, the original algorithm only used cloud liquid water path to account for cloud effects to the SDLW. For the SGP and TWP site, the effect of ice clouds on the SDLW is relatively small since most of the ice clouds are at high altitudes. Such is not the case for the polar region, where most of the clouds are ice cloud located at

low altitudes. Moreover, since the atmospheric water vapor concentrations for the Polar Regions are also very low, the effect of ice clouds on SDLW is not negligible.

3. Satellite Implementation

3.1 Data

The CERES Single Scanner Footprint (SSF) product contains one hour of instantaneous CERES data for a single scanner instrument. The SSF product combines instantaneous CERES data with scene information and cloud properties derived from a high spatial resolution imager such as the Visible/Infrared Scanner (VIRS) on TRMM or the Moderate-Resolution Imaging Spectroradiometer (MODIS) on Terra and Aqua satellites. The cloud properties are computed in the cloud subsystem of CERES processing [Minnis et al. 1997]. Thus, all of the input parameters for the Zhou-Cess algorithm are already computed or assembled in the current SSF processing.

The ground measurements are taken from the CERES/ARM Validation Experiment [CAVE; Rutan et al. 2001] database which is maintained at NASA LaRC in a Web-accessible form for use in the CERES project and is available to the outside science community. The surface observations used in this study include 5 ARM/SGP sites, 1 ARM/TWP site, 7 National Surface Radiation Budget Network (SURFRAD; Augustine et al., 2000) sites, 8 Baseline Surface Radiation Network [BSRN; Ohmura et al. 1998] sites, 6 Climate Monitoring and Diagnostics Laboratory (CMDL) sites, the LARC/COVE site [Jin et al., 2002], and one NREL [Myers et al. 1999] site (Fig. 4). These sites were selected based on data availability and statistical representative of different geographical regions, i.e., ocean, land, desert, arctic regions. Temporal matching of the satellite and

site fluxes was done at the highest resolution of the site data. Spatial matching was done to a distance of 10 km between the location of the site and the center of the CERES footprint. Values for all CERES footprints within the 10 km range of the sites and within the 1 minute interval were averaged together for comparison with the corresponding ground-based values.

For the purpose of deriving, as well as validating, a new algorithm, it is necessary to separate the training and validating data set. Here we have chosen 15 ground stations and collocated cloud parameters from Terra satellite during 58 months from March 2000 to Dec 2004 as a training data set. All 29 ground stations and their collocated Terra products for the same period are used in the validation since only clear and overcast portions of the training data set are used in the derivation of the algorithm. The collocated Aqua and ground measurements from all 29 stations covering the period from July 2002 to March 2005 serve as additional data set for validation.

3.2 Performance of the original algorithm

Fig. 5 shows the scatter plots of SDLW computed by the original Zhou-Cess algorithm for Terra satellite and collocated ground measurements from all 29 sites. For most geographical regions (continental, desert, island and coastal area), the algorithm performs reasonably well; however, there is a significant underestimation of the SDLW in the Ant(arctic), which is defined to include both the Arctic and Antarctic, when SDLW is below 200 Wm^{-2}. Most of the low values were observed at the South Pole where mean water vapor is only 0.34 cm. When the data are stratified with clear ($f_{clr} > 0.999$), water cloud (LWP > 5 g/m^2) and ice cloud (LWP < 5 g/m^2 and ice water path (IWP) > 1 g/m^2)

cases, we find that there is positive bias for most of the clear sky cases except in some Ant(arctic) cases (Fig. 6). Large negative bias was found for both water cloud and ice cloud, with ice clouds having the largest negative bias. The large negative bias for cloudy sky flux might be due to lower cloud liquid water path generally observed from satellite than those observed from MWR at the SGP site. The PDFs of Fig. 7 show that the satellite rarely observes LWP greater than 1 mm over the SGP site while MWR observe many cases with LWP greater than 1 mm. We also found that some of the MWR measured cloud liquid water used in deriving the original algorithm might have been contaminated by rain or wetness from other forms of precipitation due to their unlikely larger value (LWP > 1.3 mm). The systematic difference between ice cloud and water cloud also indicates that ice clouds can play an important role for conditions other than the warm, moist tropical conditions. Taken together, these observations suggest that the algorithm should be re-derived using satellite observed cloud parameters and using more sites globally so that the algorithm better represents of various atmospheric conditions. In the revised algorithm, the effect of ice cloud will be considered by including ice water content in the same manner as cloud liquid water although with a smaller weight.

3.3. Revised algorithm

Based on the above analysis, a new algorithm was formulated which computes the fluxes for clear portions (F_{clr}) and cloudy portions (F_{cld}) of the sky separately and then sums the results for the all sky flux (F_{all}):

$$F_{clr} = a0 + a1 \cdot SULW + a2 \cdot ln(1 + PWV) + a3 \cdot [ln(1 + PWV)]^2 \qquad (2)$$

$$F_{cld} = b0 + b1 \cdot SULW + b2 \cdot ln(1 + PWV) + b3 \cdot [ln(1 + PWV)]^2 +$$

$$b4 \bullet ln(1 + LWP) + b5 \bullet ln(1+IWP) \quad (3)$$

$$F_{all} = F_{clr} \bullet f_{clr} + F_{cld} \bullet (1.0 - f_{clr}) \quad (4)$$

$$F_{net} = F_{all} - SULW \quad (5)$$

a0 = 37.687, a1 = 0.474, a2 = 94.190, a3 = -4.935

b0 = 60.349, b1 = 0.480, b2 = 127.956,

b3 = -29.794, b4= 1.626, b5 = 0.535

where f_{clr} is the fraction of clear area in a single CERES footprint. SULW and PWV follow the same units as in (1). LWP and IWP (in g/m^2) are not representative of the total for the pixel, but only for the cloudy portion, since the cloud fraction is explicitly taken into consideration. The cloud fraction and cloud water path are part of SSF product and derived from CERES cloud analysis. The column precipitable water vapor is integrated from CERES meteorological data. Moreover, clear sky is defined when f_{clr} is greater than 0.999 and both LWP and IWP are set to zero. SULW is computed using a surface skin temperature with an emissivity of unity. Test cases run to incorporate a global emissivity map demonstrated no improvement in the algorithm.

As noted previously, the above regressions are derived using satellite observations from the Terra platform and matched ground measurements from 15 sites around the globe (Fig. 4) from March 2000 to Dec 2004. There are 6028 clear sky cases ($f_{clr} > 0.999$) for deriving the clear sky formula and 5788 overcast cases ($f_{clr} < 0.01$) for the cloudy sky formula. These data consist of 43% of all collocated measurements in the training data set.

3.4. Validation

The modified algorithm has been applied to the CERES Terra Edition 2B and Aqua Edition 2A SSF data products. The Terra Edition 2B data, as mentioned previously, spans from the period from March 2000 to December 2004. The Aqua Edition 2A data covers the period from July 2002 to March 2005. Fig.8 illustrates the comparison of the SDLW of Terra Edition 2B computed with the modified Zhou-Cess algorithm versus the ground measured SDLW over 29 sites around the globe stratified for different scene types. The modified algorithm has smaller bias (less than 1 Wm^{-2}) than the original algorithm for most of the scene types except for the coastal scenes where the systematic bias is 7.3 Wm^{-2}. The scatter plots in Fig. 9 of the derived versus measured SDLW shows that the systematic bias from water cloud and ice cloud are both reduced and the difference between them is also reduced as compared to those from the original algorithm shown in Fig. 6.

The modified algorithm (named LW model C or LWC here) has also been applied to Aqua processing along with LWA and LWB, with the following results covering the 33 months from July 2002 to March 2005. The ground measurements are collected from the same 29 global sites as shown in Fig. 4. All data available from these periods are used except for some data gaps. The validation was carried for clear sky and cloudy sky separately.

Table 1 compares the bias and random error of the original algorithm to those of the modified algorithm as well as LWA and LWB for clear sky fluxes. Using the modified algorithm reduces the huge negative bias for the (Ant)arctic region from -137.0 Wm^{-2} to an acceptable -10.5 Wm^{-2}. The use of the modified algorithm has also resulted in improvement to either the bias or random error or both for most of the regions. The

modified algorithm does produce biases for coastal and (Ant)arctic areas of the order of 10 Wm^{-2}, whereas globally, there is a less than 1 Wm^{-2} bias and an 18 Wm^{-2} random error. Comparison of LWC with LWA and LWB for clear sky fluxes shows that the modified LWC has smaller bias for continental region than both LWA and LWB. LWC does, however, have larger systematic bias in the coastal and desert areas. The global mean bias is smaller for LWC probably due to cancellation of positive and negative biases. The random error of 18.5 Wm^{-2} is slightly higher than those of LWA (17. 7 Wm^{-2}) and LWB (16.8 Wm^{-2}).

Table 2 compares the bias and random error of the original algorithm to those of the modified algorithm as well as LWB for cloudy sky fluxes (LWA only computes clear sky flux). The results in Table 2 show that the major improvement for cloudy sky flux also occurs at (Ant)arctic region. The bias is reduced from -46.6 Wm^{-2} to -0.89 Wm^{-2}. There is also a modest improvement for the continental areas, though the bias is slightly larger for coastal and desert regions. Globally, the bias is 1.2 Wm^{-2} with a random error of 23.6 Wm^{-2}. Comparing LWC cloud sky flux with LWB, we find that LWC performs slightly better in continental, (Ant)arctic, desert and island regions, while only slightly worse in coastal areas.

Similar results for all sky fluxes (clear plus cloudy cases) are shown in Table 3. The modified algorithm shows improvements over original algorithm for most geographical regions in systematic error, except for coastal and island regions. Meanwhile, the random error is reduced for every region. The modified LWC has slightly smaller systematic bias than LWB for all the regions except for the coastal region, which still has a systematic bias of 6.6 Wm^{-2}. The global mean bias of all sky fluxes is 1.1 Wm^{-2}

and the random error is 23.0 Wm^{-2}, slightly better than LWB. Although LWC and LWB are very different algorithms, we have observed that the random errors of both models are fairly close to each other for each geographical region. This might be related with spatial temporal collocation of satellite measurements with ground measurements and the uncertainties associated with satellite retrieved cloud parameters, i.e., cloud fraction used in both algorithms.

Despite the overall good performance, there are a few regions or stations that still present large biases. It is found that the large bias of coastal area mainly comes from the COVE (Chesapeake light house, 36.90° N, 75.71° W) site which has a positive bias of 18.6 Wm^{-2}. Besides the COVE site, a few other sites, namely, Fort Peck (FPK, 48.31° N, 105.10° W), Sioux Falls (SXF, 43.73° N, 96.92° W), Payerne (PAY, 46.82° N, 6.95° E) and the South Pole (SPL) have systematic bias larger than 10 Wm-2. The causes for the large biases in these sites maybe related with specific conditions of the sites and should be examined individually.

Gupta et al. [2004] found that systematic bias of LWB varies with instrument network and day-night skin temperature bias. To rule out that some of the systematic bias might be due to instrument setup, we computed the biases grouped with different network. Table 4 shows no discernible trends in systematic bias between different networks. The ARM instruments have smaller random error because four out of five instruments are clustered in the ARM SGP site. The BSRN instruments have the largest random error due to varied geographical locations of the measurements. The small systematic bias should not be contributed to instruments themselves.

The systematic differences between daytime and nighttime biases, however, are found for all sky fluxes from both Terra and Aqua platforms (Table 5). The revised algorithm overestimates the daytime SDLW by 3-4 Wm^{-2} and underestimates nighttime SDLW by 2-3 Wm^{-2}. This might be related to the use of skin temperature estimates. The original algorithm uses 2-meter air temperature which is more closely related to the lower atmosphere and hence the SDLW. An investigation is currently underway at NASA Langley Research Center to use a constrained surface temperature in the CERES surface radiation product since all of the LW models tend to overestimate the surface downward LW radiation for cases where the surface temperatures are significantly higher than the air temperatures. The modified skin temperature (or constrained temperature) is expected to reduce the day-night bias and also the overall bias in this algorithm and others.

4. Conclusions

An improved version of Zhou-Cess algorithm has been formulated which avoids the large errors in the SDLW at low water vapor conditions by adding an offset to the logarithmic water vapor term. The new algorithm also utilizes cloud fraction and cloud liquid and ice water paths available from the CERES SSF product to separately compute the clear and cloudy portions of the flux. The new algorithm has been validated for the Terra and Aqua satellites against surface measurements at 29 stations around the globe. The results show significant improvement over the original version and are comparable or slightly better than the more sophisticated algorithms currently implemented in the CERES processing. This revised version of Zhou-Cess algorithm will be incorporated into the CERES operational processing.

Acknowledgements: The first author is supported by NASA Interdisciplinary Research in Earth Science NRA-02-OES-06 under WBS 509496.02.01.01.07, UPN 291-01-97-05 and UPN 291-01-c7 and is much grateful to Dr. Arthur. Y. Hou for his support and Dr. Warren Wiscombe for his insightful comments of the manuscript. The CERES SRB project is sponsored by WBS 921266.04.07.07. ARM data is made available through the U.S. Department of Energy as part of the Atmospheric Radiation Measurement Program.

REFERENCES

Augustine, J. A., J. J. DeLuisi, and C. N. Long, 2000: SURFRAD-A National Surface Radiation Budget Network for Atmospheric Research, Bull. of Amer. Met. Soc. Vol. 81, No. 10, pp. 2341-2358.

Charlock, T. P., and Coauthors (1997): Compute surface and atmospheric fluxes (system 5.0): CERES Algorithm Theoretical Basis Document Release 2.2), NASA/RP-1376, 84 pp. [Available online at asd-www.larc.nasa.gov/ATBD/ATBD.html.].

Darnell, W. L., W. F. Staylor, S. K. Gupta, N. A. Ritchey, and A. C. Wilber, 1992: Seasonal variation of surface radiation budget derived from ISCCP-C1 data. *J. Geophys. Res.*, **97**, 15741–15760.

Gupta, S. K., W. L. Darnell, and A. C. Wilber, 1992: A parameterization for longwave surface radiation from satellite data: Recent improvements. *J. Appl. Meteor.*, **31**, 1361–1367.

Gupta, S. K., D. P. Kratz, A. C. Wilber, and L. C. Nguyen, 2004: Validation of Parameterized Algorithms Used to Derive TRMM–CERES Surface Radiative Flux. *J. Atmos. Ocea. Tech.*, 21, 742–752.

Hack, J. J., Sensitivity of the simulated climate to a diagnostic formulation for cloud l iquid water, *J. Climat., 11*, 1497-1515, 1998.

Inamdar, A. K., and V. Ramanathan, 1997: On monitoring the atmospheric greenhouse effect from space. *Tellus.*, **49B**, 216–230.

Jin, Z., T. P. Charlock, and K. Rutledge, 2002: Analysis of the Broadband Solar Radiation and Albedo Over the Ocean Surface at COVE. J. Atmos. & Ocean Tech. 19, pp. 1585-1601.

Li, Z., H. G. Leighton, and R. D. Cess, 1993: Surface net solar radiation estimated from satellite measurements: Comparisons with tower observations. *J. Climate.*, **6**, 1764–1772.

Minnis, P., and Coauthors, 1997: Cloud optical property retrieval (system 4.3). CERES Algorithm Theoretical Basis Document (Release 2.2), NASA/RP-1376, 60 pp. [Available online at asd-www.larc.nasa.gov/ATBD/ATBD.html.].

Myers, D. R., S. Wilcox, M. Anderberg, S. H. Alawaji, N. M. Al Abbadi, M. Y. bin Mahfoodh, 1999: Saudi Arabian solar radiation network of data for validating satellite remote-sensing systems, Earth Obs. Sys. IV SPIE Vol 3750, 18-20 July, Denver CO.

Ohmura A., E. Dutton, B. Forgan, C. Frohlich, H. Gilgen, H. Hegne, A., Heimo, G., Konig-Langlo, B. McArthur, G. Muller, R. Philipona, C. Whitlock, K. Dehne, and M. Wild, 1998: Baseline Surface Radiation Network (BSRN/WCRP): New precision radiometery for climate change research. Bull. Amer. Meteor. Soc., Vol. 79, No. 10, 2115-2136.

Rutan, D.A., F.G. Rose, N.M. Smith, T.P. Charlock, 2001: Validation data set for CERES surface and atmospheric radiation budget (SARB), WCRP/GEWEX Newsletter, Vol 11, No. 1, 11-12. [Available online at www.gewex.org/feb01.pdf; data available online at www-cave.larc.nasa.gov/cave/.].

Stamnes, K., R. G. Ellingson, J. A. Curry, J. E. Walsh and B. D. Zak. 1999: Review of Science Issues, Deployment Strategy, and Status for the ARM North Slope of Alaska–Adjacent Arctic Ocean Climate Research Site. *J. Climat.*, 12, 46–63.

Stokes, G. M., and S. E. Schwartz, 1994: The Atmospheric Radiation Measurement (ARM) program: Programmatic background and design of the cloud and radiation testbed. *Bull. Amer. Meteor. Soc.,* **75**, 1201–1221.

Wang, J. G. P. Anderson, H. E. Revercomb, and R. O. Knutson (1996), Validation of FASCOD3 and MODTRAN3: Comparison of model calculations with ground-based and airborne interferometer observations under clear-sky conditions. *Appl. Opt. 65*, 6028–6040.

Wielicki, B. A., B. R. Barkstrom, E. F. Harrison, R. B. Lee III, G. L. Smith, and J. E. Cooper, 1996: Clouds and the Earth's Radiant Energy System (CERES): An Earth Observing System experiment. *Bull. Amer. Meteor. Soc.,* **77**, 853–868.

Zhou, Y. P., and R. D. Cess, 2001:Algorithm development strategies for retrieving the downwelling longwave flux at the Earth’s surface. J. Geophys. Res., 106, 12,477-12,488.

Table 1. Error statistics of longwave clear sky fluxes computed from LWC (original LWC, modified LWC), LWA and LWB against surface measurements for Aqua satellite from July 2002-March 2005.

Sites # of Points		Original LWC	LWC	LWA	LWB
Continental 5012	Bias Wm^{-2} (%) σ Wm^{-2} (%)	6.71 (2.38) 20.9 (7.4)	-0.16(-0.06) 16.6 (5.9)	-4.48(-1.59) 15.8 (5.6)	-6.93(-2.46) 15.4 (5.5)
Coastal 609	Bias Wm^{-2} (%) σ Wm^{-2} (%)	16.66 (5.84) 17.8 (6.3)	10.03(3.52) 14.8 (5.2)	4.92 (1.72) 12.9 (4.5)	-0.15(-0.05) 13.2 (4.6)
Ant(arctic) 903	Bias Wm^{-2} (%) σ Wm^{-2} (%)	-137.0(122.0) 34.5 (30.7)	10.45(9.30) 11.1 (9.9)	-16.0(14.30) 11.0 (9.9)	-8.83(-7.88) 11.0 (9.9)
Desert 1640	Bias Wm^{-2} (%) σ Wm^{-2} (%)	-1.68 (-0.53) 24.4 (7.8)	-7.12(-2.27) 23.9 (7.6)	-0.41 (-0.13) 22.8 (7.3)	-5.15 (-1.64) 21.1 (6.7)
Island 138	Bias Wm^{-2} (%) σ Wm^{-2} (%)	9.31 (2.47) 10.3 (2.7)	2.92(0.77) 12.6 (3.3)	-0.75 (-0.20) 12.0 (3.2)	-0.77 (-0.20) 13.8 (3.6)
Global 8302	Bias Wm^{-2} (%) σ Wm^{-2} (%)	-9.81 (-3.61) 41.4 (15.3)	0.42 (0.15) 18.5 (6.8)	-4.18 (-1.54) 17.7 (6.5)	-6.19 (-2.28) 16.8 (6.2)

Table 2. Error statistics of long wave cloudy sky flux computed using LWC (original, modified) and LWB against surface measurements for Aqua satellite from July 2002-March 2005.

Sites # of Points		Original LWC	LWC	LWB
Continental 21117	Bias Wm^{-2} (%) σ Wm^{-2} (%)	-7.42 (-2.33) 28.0 (8.8)	0.61 (0.19) 22.6 (7.1)	-3.38 (-1.06) 22.4 (7.0)
Coastal 3302	Bias Wm^{-2} (%) σ Wm^{-2} (%)	1.80 (0.52) 21.2 (6.1)	6.00 (1.72) 18.5 (5.3)	2.51 (0.72) 19.0 (5.4)
Ant(arctic) 17663	Bias Wm^{-2} (%) σ Wm^{-2} (%)	-46.63 (-20.17) 50.6 (21.9)	-0.89 (-0.39) 23.6 (10.2)	-6.17 (-2.67) 25.0 (10.8)
Desert 4170	Bias Wm^{-2} (%) σ Wm^{-2} (%)	8.19 (2.42) 28.1 (8.3)	9.67 (2.85) 27.7 (8.2)	11.88 (3.51) 28.8 (8.5)
Island 6729	Bias Wm^{-2} (%) σ Wm^{-2} (%)	0.58 (0.14) 13.5 (3.3)	0.95 (0.23) 12.5 (3.0)	5.71 (1.39) 14.8 (3.6)
Global 52981	Bias Wm^{-2} (%) σ Wm^{-2} (%)	-17.67 (-5.80) 40.1 (13.2)	1.20 (0.39) 23.6 (7.8)	-1.59 (-0.52) 24.4 (8.0)

Table 3. Error statistics of long wave all sky flux computed using LWC (original, modified) and LWB against surface measurements for Aqua satellite from July 2002-March 2005.

Sites # of Points		Original LWC	LWC	LWB
Continental 26129	Bias Wm^{-2} (%) σ Wm^{-2} (%)	-4.71 (-1.51) 27.2 (8.7)	0.46 (0.15) 21.6 (6.9)	-4.06 (-1.31) 21.3 (6.8)
Coastal 3911	Bias Wm^{-2} (%) σ Wm^{-2} (%)	4.12 (1.21) 20.9 (6.1)	6.63 (1.95) 18.1 (5.3)	2.10 (0.62) 18.4 (5.4)
Ant(arctic) 18566	Bias Wm^{-2} (%) σ Wm^{-2} (%)	-51.03 (-22.64) 51.6 (22.9)	-0.34 (-0.15) 23.3 (10.3)	-6.30 (-2.79) 24.8 (11.0)
Desert 5810	Bias Wm^{-2} (%) σ Wm^{-2} (%)	5.40 (1.63) 27.5 (8.3)	4.93 (1.48) 27.4 (8.3)	7.08 (2.13) 27.3 (8.2)
Island 6867	Bias Wm^{-2} (%) σ Wm^{-2} (%)	0.76 (0.19) 13.5 (3.3)	0.99 (0.24) 12.5 (3.1)	5.58 (1.36) 14.8 (3.6)
Global 61283	Bias Wm^{-2} (%) σ Wm^{-2} (%)	-16.61 (-5.54) 41.1 (13.7)	1.09 (0.36) 23.0 (7.7)	-2.22 (-0.74) 23.5 (7.8)

Table 4. Bias of long wave all sky fluxes computed using LWC compared with surface measurements stratified with observational network.

Platform		ARM	SURF	BSRN	CMDL
Terra	Bias Wm^{2}	1.1	2.9	-3.1	0.5
	σ Wm^{-2}	17.6	22.2	26.2	21.2
Aqua	Bias Wm^{-2}	2.7	0.9	-0.2	-1.1
	σ Wm^{-2}	18.8	22.6	27.6	21.1

Table 5. Bias of long wave all sky fluxes computed using LWC compared with surface measurements stratified with observational time.

		Daytime	Nighttime
Terra	Bias Wm^2	4.9	-3.4
	σ Wm^{-2}	15.7	24.3
Aqua	Bias Wm^2	3.5	-2.3
	σ Wm^{-2}	20.9	24.2

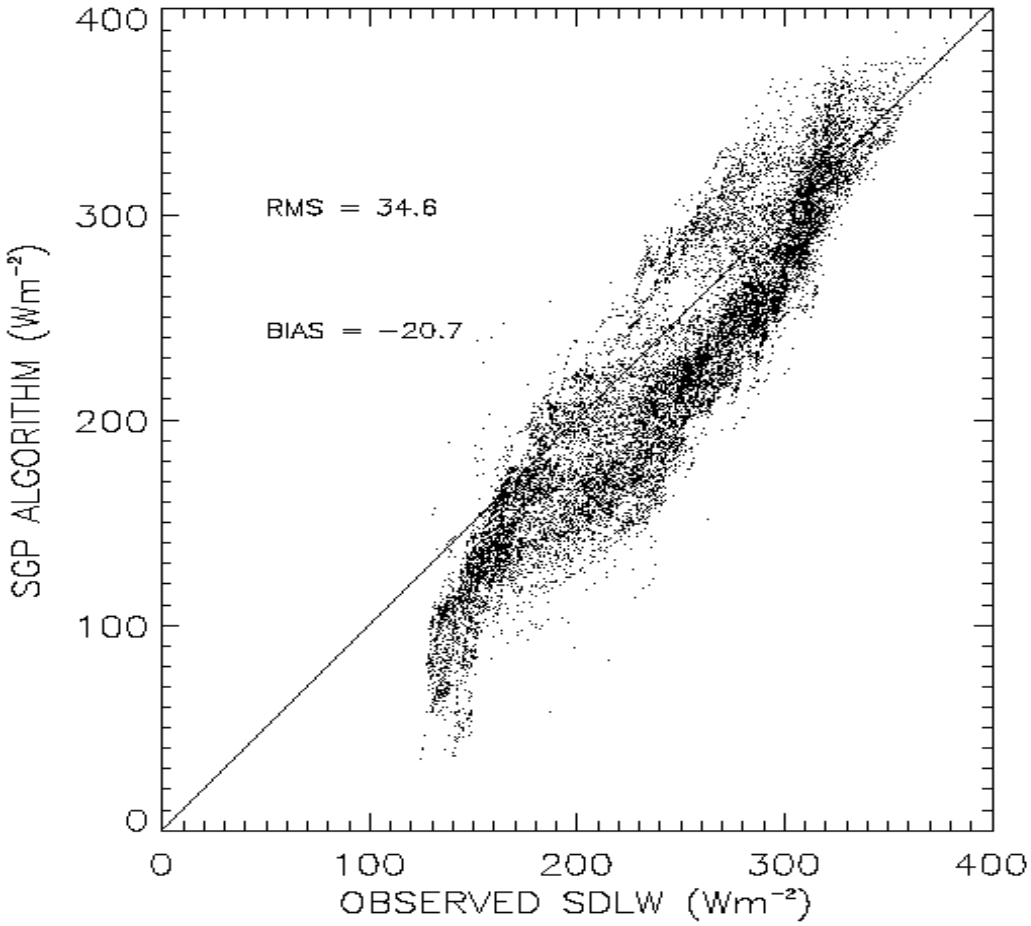

Fig. 1 Scatter plot of observed SDLW versus SDLW calculated with original Zhou-Cess algorithm for ARM data from Barrow, NSA from Jan.2000-Dec.2000.

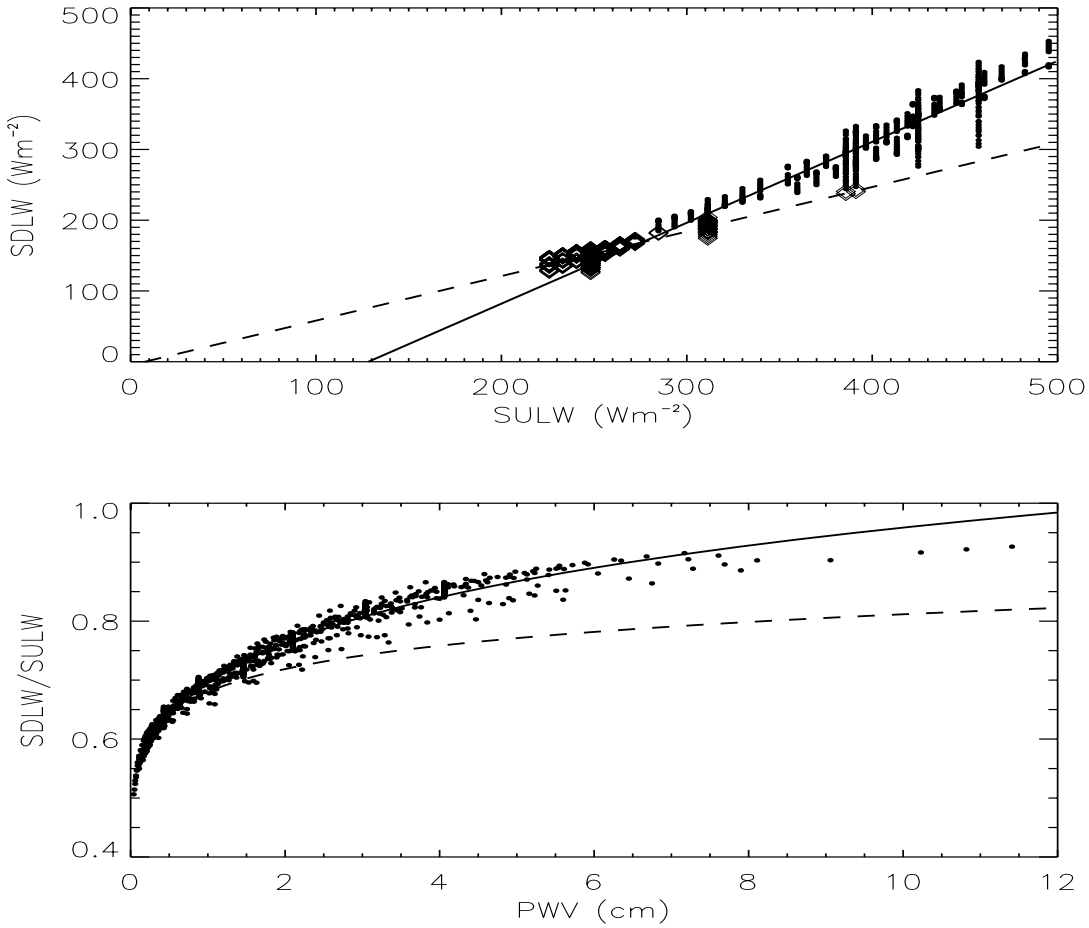

Fig. 2 Relationships between MODTRAN computed clear sky SDLW and SULW (upper panel) and flux ratio versus column water vapor (lower panel). The black and dot lines are linear regression fits (upper panel) and log-square fits (lower panel) using data points with PWV greater than 0.5 cm (solid line) and PWV less than 0.5 cm (dot lines), respectively.

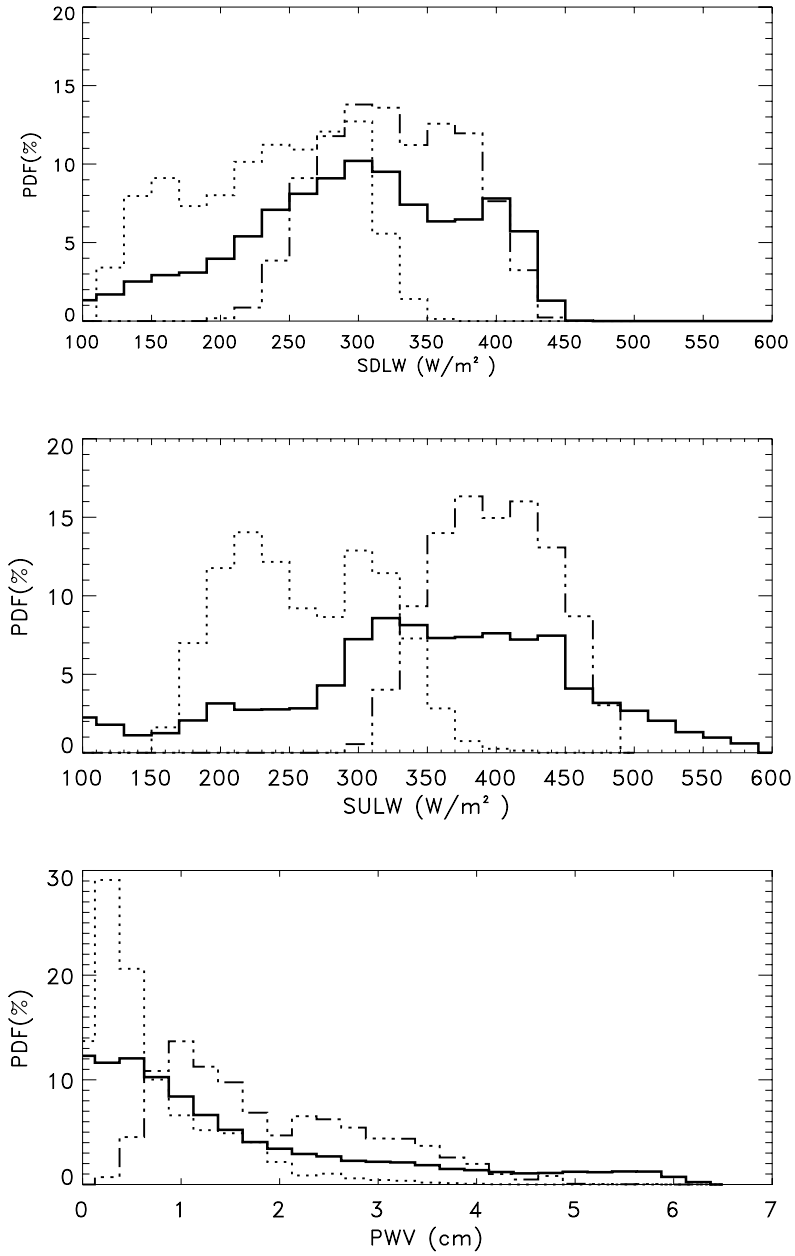

1

2 Fig. 3 Normalized probability distribution functions of SDLW, SULW and PWV from

3 global network (solid line), ARM SGP site (dash-dot line) and ARM NSA site (dot line).

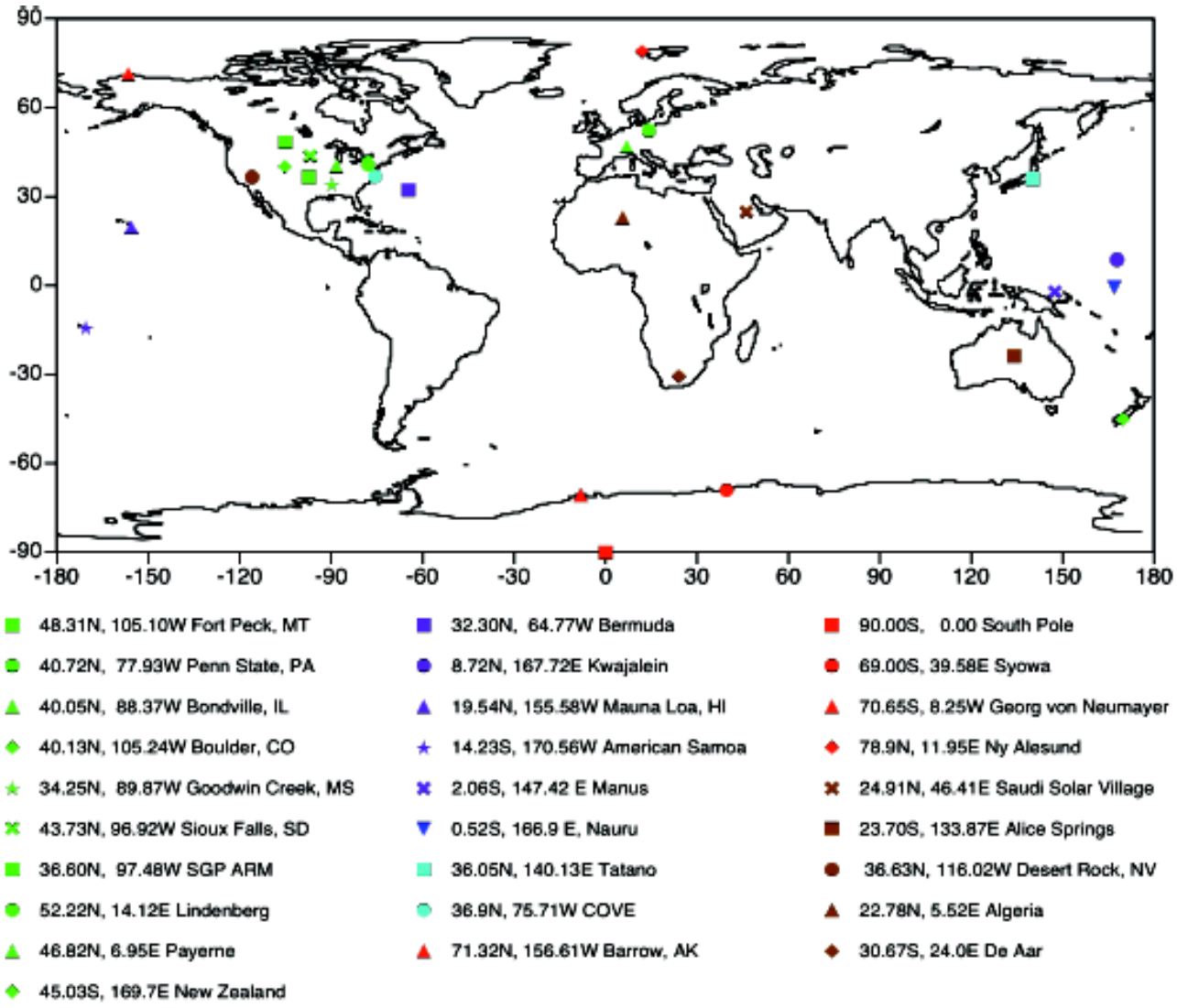

Fig. 4 Ground stations used in this study.

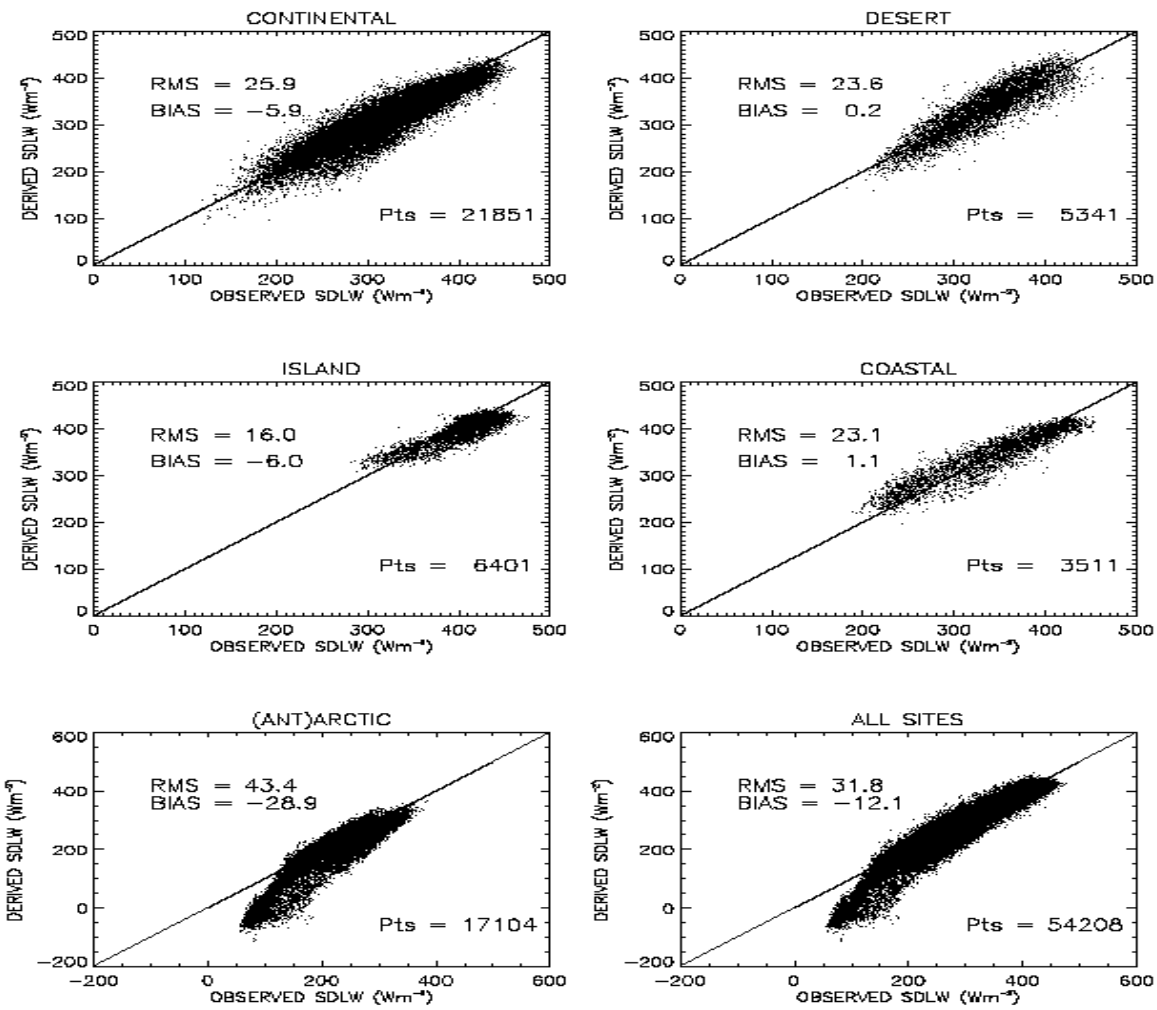

1

2

3 Fig. 5 Scatter plots of SDLW computed using original Zhou-Cess algorithm for Terra

4 satellite versus ground measurements for different scene types.

5

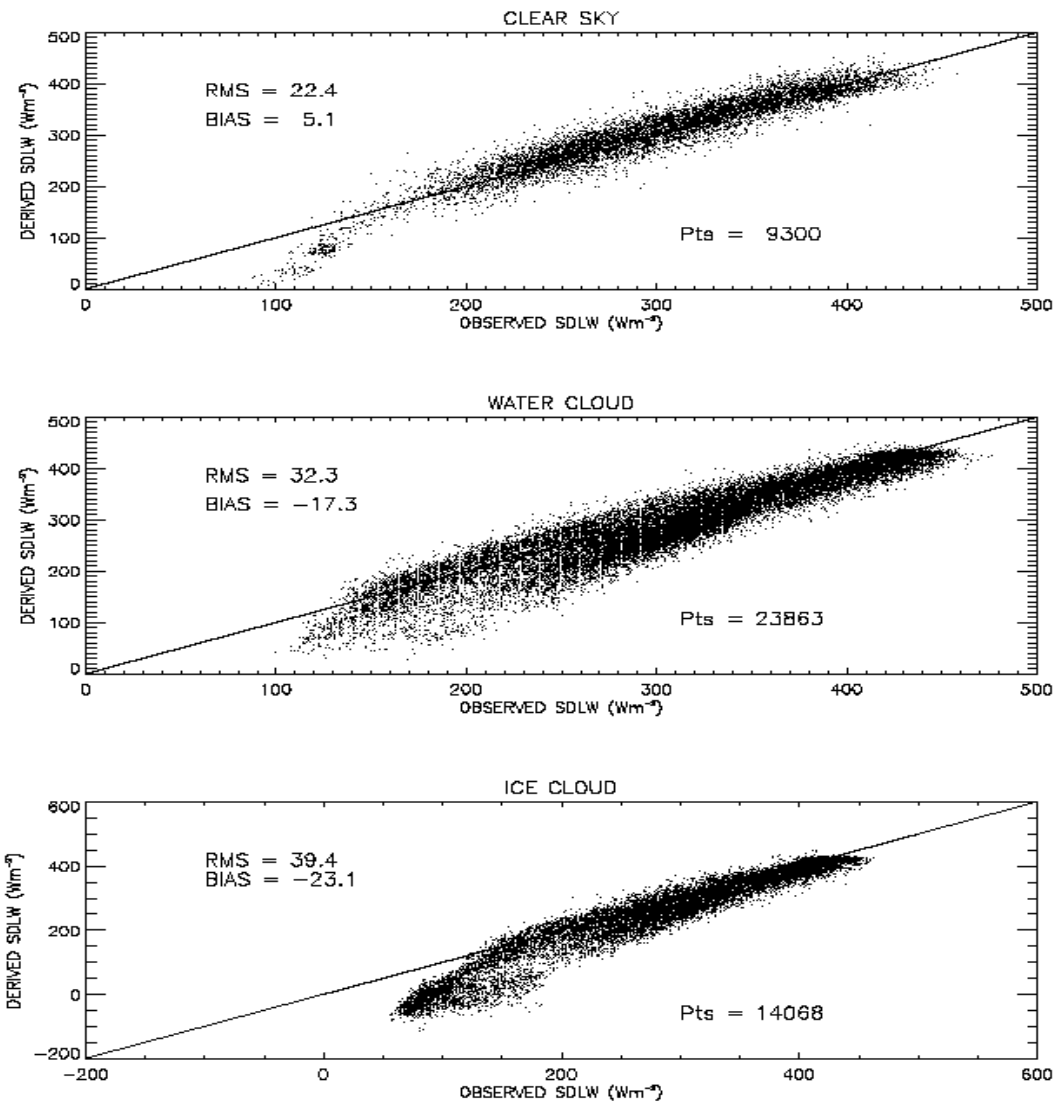

1

2 Fig. 6 Scatter plots of SDLW computed using original Zhou-Cess algorithm versus
3 ground measurements stratified for clear sky (Area_clr > 99.9%), water cloud (LWP>5
4 g/m^2) and ice cloud (LWP < 5 g/m^2, IWP>1 g/m^2) conditions for Terra satellite.

5

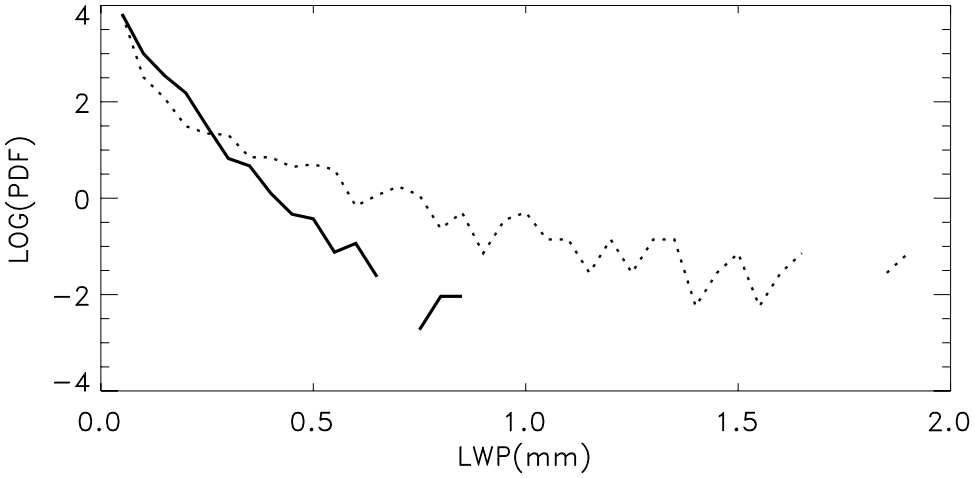

1

2

3 Fig.7 Logarithmic normalized probability distribution functions of cloud liquid water
4 path from ARM SGP site as observed from ARM microwave radiometer (dotted line) and
5 CERES instruments (solid line).

6

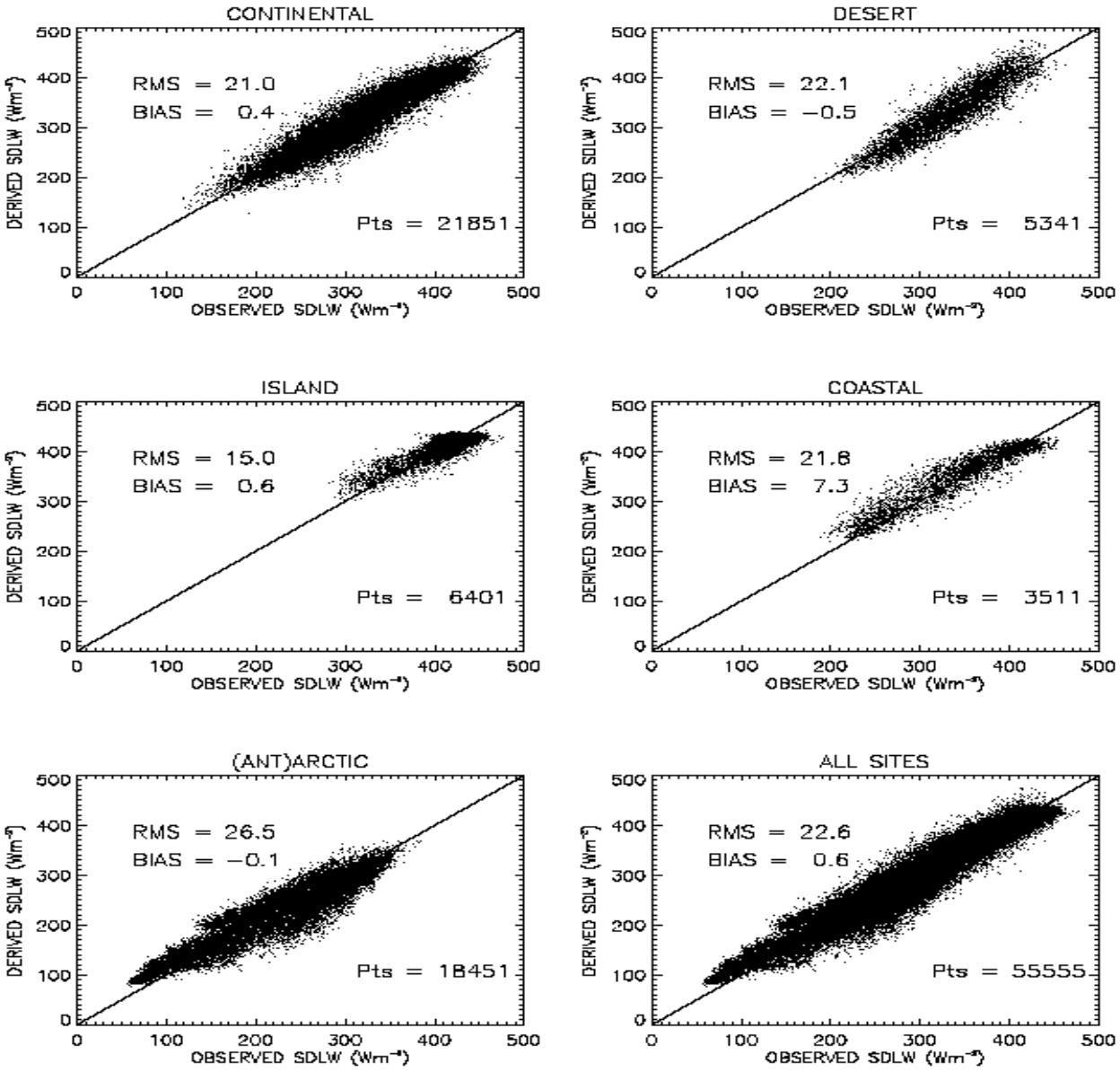

Fig. 8 Scatter plots of SDLW computed using modified Zhou-Cess algorithm versus ground measurements for different scene types for Terra satellite from March 2000 to December 2004.

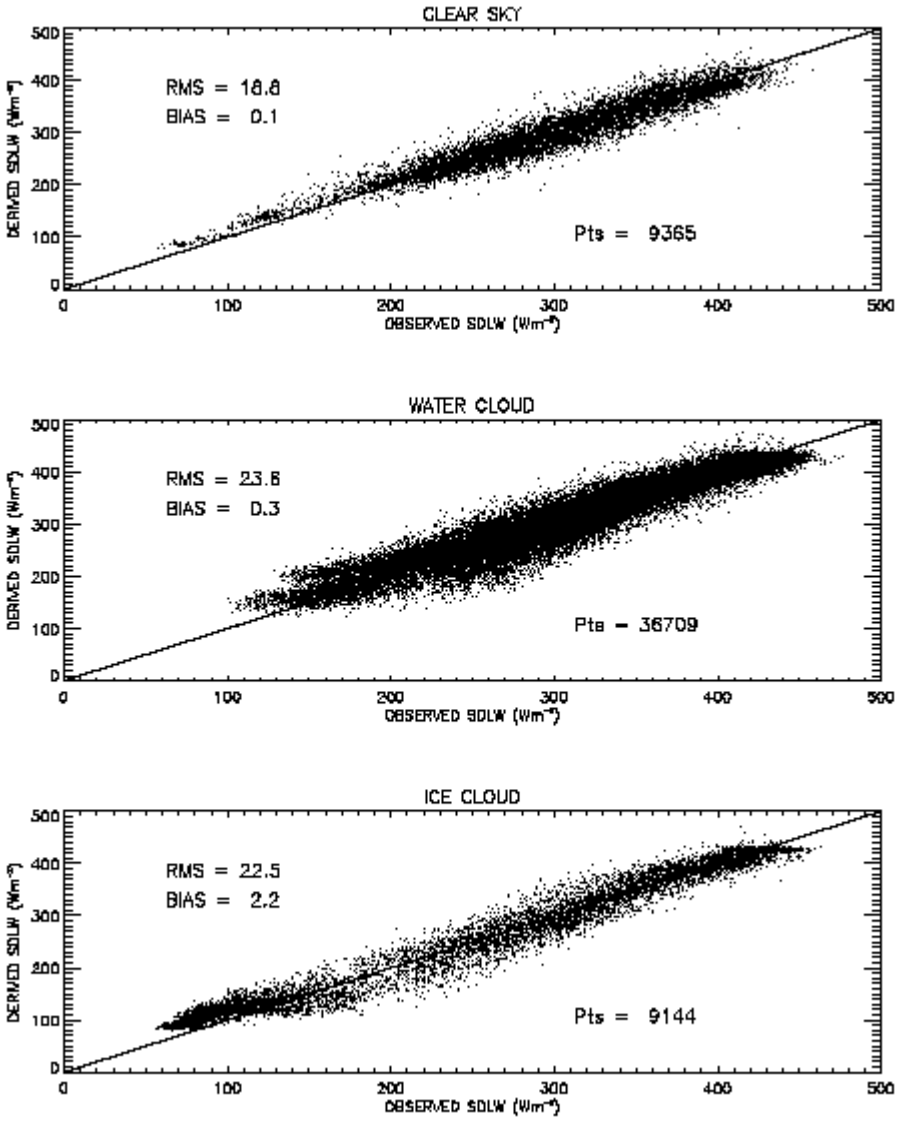

1

2 Fig. 9 Scatter plots of SDLW computed using modified Zhou-Cess algorithm versus
3 ground measurements stratified for clear sky (Area_clr > 99.9%), water cloud (LWP>5
4 g/m^2) and ice cloud (LWP < 5 g/m^2, IWP>1 g/m^2) conditions for Terra satellite from
5 March 2000 to December 2004.

6